SCIENTIFIC REPORTS

OPEN

SUBJECT AREAS:
APPLIED PHYSICS
BIOLOGICAL PHYSICS

Received
1 August 2013

Accepted
16 October 2013

Published
31 October 2013

Correspondence and requests for materials should be addressed to J.-S.W. (wangjs@tju.edu.cn) or X.-Q.F. (fengxq@tsinghua.edu.cn)

Hierarchical chirality transfer in the growth of *Towel Gourd* tendrils

Jian-Shan Wang[1,2], Gang Wang[3], Xi-Qiao Feng[4], Takayuki Kitamura[2], Yi-Lan Kang[1], Shou-Wen Yu[4] & Qing-Hua Qin[5]

[1]Tianjin Key Laboratory of Modern Engineering Mechanics, Department of Mechanics, Tianjin University, Tianjin 300072, People's Republic of China, [2]Department of Mechanical Engineering and Science, Kyoto University, Nishikyo-ku, Kyoto 615-8540, Japan, [3]School of Materials Science and Engineering, Shanghai University, Shanghai 200444, People's Republic of China, [4]AML and CNMM, Department of Engineering Mechanics, Tsinghua University, Beijing 100084, People's Republic of China, [5]Research School of Engineering, Australian National University, Canberra, ACT 0200, Australia.

Chirality plays a significant role in the physical properties and biological functions of many biological materials, e.g., climbing tendrils and twisted leaves, which exhibit chiral growth. However, the mechanisms underlying the chiral growth of biological materials remain unclear. In this paper, we investigate how the *Towel Gourd* tendrils achieve their chiral growth. Our experiments reveal that the tendrils have a hierarchy of chirality, which transfers from the lower levels to the higher. The change in the helical angle of cellulose fibrils at the subcellular level induces an intrinsic torsion of tendrils, leading to the formation of the helical morphology of tendril filaments. A chirality transfer model is presented to elucidate the chiral growth of tendrils. This present study may help understand various chiral phenomena observed in biological materials. It also suggests that chirality transfer can be utilized in the development of hierarchically chiral materials having unique properties.

Many biological materials, such as climbing plant tendrils[1,2], flower petals of *Paphiopedilum dianthum*[3], and snail shells[4], exhibit chiral growth. In these natural materials, there are a number of distributed chiral elements, e.g., biomacromolecules, which lead to the formation of various chiral morphologies and surface patterns at the macroscopic scale. For example, helices and twisted belts are often observed to form in growing biological materials. These chiral morphologies generally tend to a specific handedness, either right or left[5]. A well-known example is climbing tendrils, which help some climbing plants attach to trees or other objects and to provide supporting forces[2]. The investigation of the mechanisms underlying the chiral growth of biological materials is a fundamental and important issue in not only developmental biology but also materials science and technology.

The chiral shapes of some biological and artificial materials may origin from the asymmetry of growth, deswelling[6,7], surface stresses[8,9] and other physical quantities associated with anisotropic atomic or molecular structures[10]. For example, the formation of twisting belts of *Bauhinia* seed pods[6] and chiral polymer lamellae[3] has been attributed to the anisotropy of material properties and surface stresses, respectively. From the view point of chirality transfer, the chiral morphologies of many biological materials originate from the chirality of their microscopic constituent building blocks. Typical examples include the flagellar filaments of bacteria[11–13], the flower petals of Paphiopedilumdilum dianthum[3], and the stork's bill awns[14,15]. Their chiral growth is caused by the helical arrangements of protein lattices, cortical microtubules, and tilted celluloses at the micro scale, respectively. The helical tendrils of climbing plants have attracted the interest of many scientists since the pioneering work of Charles Darwin[2]. A recent study suggested that *Cucumber* tendril coiling might be induced by the asymmetric contraction of *g*-fibers[16]. However, this mechanism does not appear to explain the predominance of left-handed or right-handed helical growth in climbing plants. Analysis of the global twining direction of climbing plants shows that the predominance of a specific chirality in the helical growth of climbing plants should be attributed to the microstructures at the subcellular level rather than the Coriolis effect[17]. In addition, previous studies revealed that the intrinsic torsion of tendril filaments drives them to form helices with a specific handedness or opposite handednesses[1,18,19]. However, the physical mechanisms underlying the intrinsic torsion of tendril filaments have rarely been discussed. Furthermore, it is still unclear how the chiralities at the molecular, microscopic, and macroscopic scales in tendrils are correlated with each other.

According to Neumann's principle of symmetry, the absence of the mirror symmetry of molecules, the arrangements of atoms and protein lattices, microstructures and even morphologies of biological materials has remarkable effects on their physical and chemical properties and functions. In the present study, we investigate, both experimentally and theoretically, how the chirality is transferred from molecules to the macroscopic morphology of tendrils. To clarify their chiral growth, a theoretical model of chirality transfer in tendril filaments is developed to correlate the chirality at the subcellular level with that at the macro scale.

Results

In the experiments, we collected mature and dry tendril helices of *Towel Gourd* as samples. Swelling and deswelling experiments of the tendril helices were first performed, and then the microstructures of their tendril filaments were observed to investigate the mechanisms of chiral growth. These experiments revealed that the shape of the tendril helices can distinctly change during swelling/deswelling. Based on these results, we use the chirality transfer mechanism to explain the shape formation and evolution of tendril filaments during their growing and swelling/deswelling processes.

When the growing tip of a tendril filament is free, the tendril normally forms a helix with a specific handedness. Most free *Towel Gourd* tendril helices we observed are left-handed. However, when a tendril filament catches a supporting object, as shown in Fig. 1, the tendril will gradually evolve into a helical shape with opposite handedness, providing an elastic spring-like support that enables the plant to climb to a sufficient height. The chiral perversion process of a tendril can be interpreted by the topological conservation law[18,19]. In both cases, tendrils assume an initial curvature induced by differential growth. The formation of a helical tendril with either a specific chirality or two opposite handednesses in two segments will be elucidated using a chirality transfer model in the sequel.

We experimentally investigated the physical origin of intrinsic torsion and the mechanisms underlying the chiral growth of tendril filaments. The samples of dry and mature *Towel Gourd* tendril helices were immersed in water for 24 hours to allow the tendril helices to fully swell. The shape parameters of the left-handed part of the swelled and deswelled tendril helix were measured for four samples, and the average results of helical radii and pitch are plotted in Figs. 2(a) and (b). Compared to the dry tendrils, the number of coils of the left-handed helical part of the fully swelled tendril samples decreased from eight to seven. The helical radii of each coil had an average increase of approximately 31.6%, and the helical pitch of each coil increased by approximately 12.1%. Moreover, the cross-sectional areas of the swelled sample increased by about 6.1% compared to those of the dry tendrils. The straight part connecting the left- and right-handed helices also exhibited a distinct increase in length (approximately 11.7%). These experiments revealed that the intrinsic chirality of the building elements, rather than simple water-induced expansion/shrinkage, causes the morphological evolution of tendril helices.

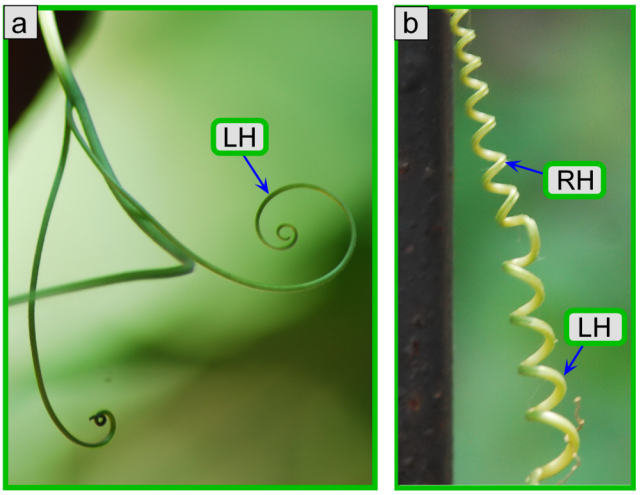

Figure 1 | *Towel Gourd* tendrils: (a) growing tendril helices without hooking and (b) tendril helices with hooking attached to a supporting object. "LH" and "RH" denote left and right handednesses, respectively.

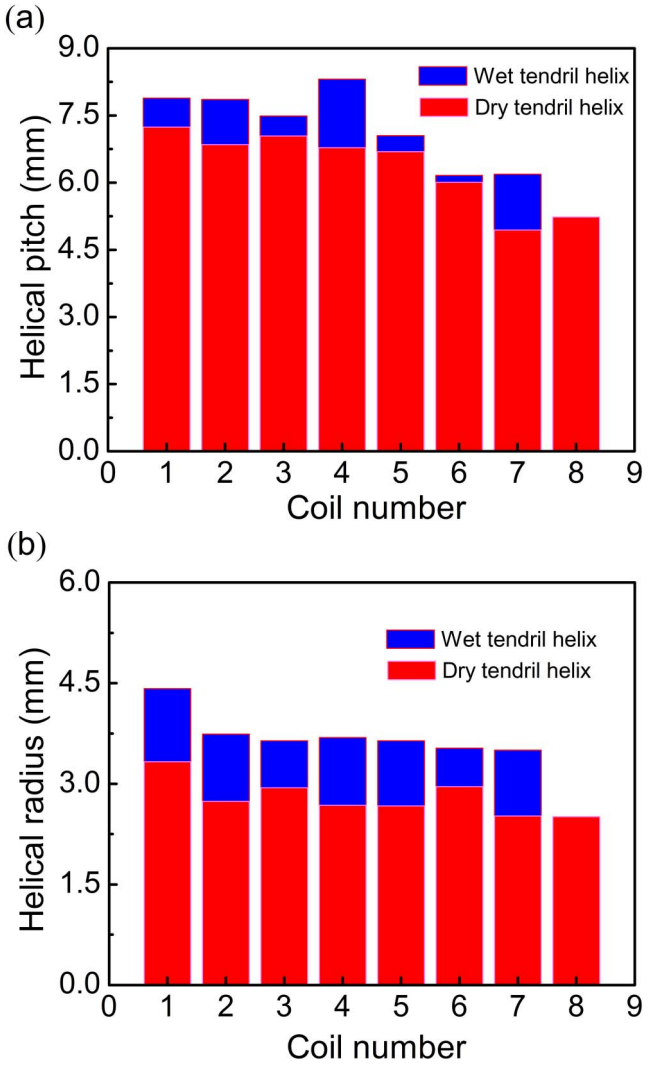

Figure 2 | Changes in (a) the helical pitches and (b) radii of tendril helices before and after swelling.

The swelled tendril helices were then placed in air for 72 hours so that they became fully deswelled. Their helical shapes returned to their initial states before swelling. Such shape changes of tendrils in the swelling/deswelling process are consistent with those of tendrils during growth. Thus they provide an ideal system to investigate the mystery of the widely observed chiral growth of natural materials.

The shape evolution of tendril helices is attributed to the changes in their microscopic structures during the swelling and deswelling processes. We observed the microstructures of tendril filaments using a scanning electron microscope (SEM). At the macro scale, a tendril filament has an approximately circular cross section with a characteristic size of 0.6–1.5 mm, containing primarily a surface layer (L1), an inner layer (L2) and a core (L3), as shown in Figure 3(a). L1 is composed of connected epidermis cells, L2 consists primarily of parallelized cells, which are tightly glued together, and L3 contains relatively large sized cells. To further study the microstructures of tendril, we cut a tendril filament into slices and observed

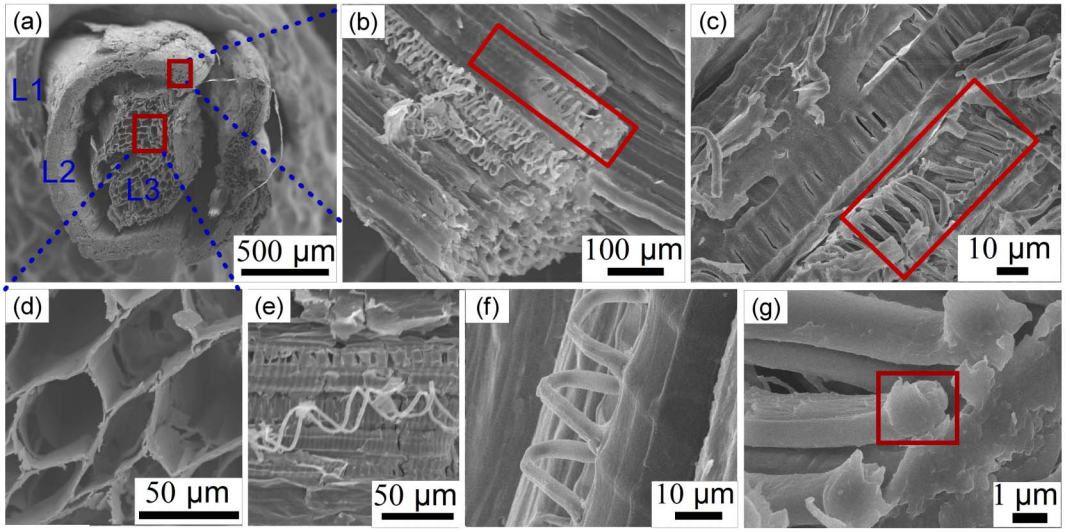

Figure 3 | Hierarchical structures of tendril filaments. (a) Cross section of a tendril filament, (b) inner layer of a tendril filament dissected longitudinally, (c) cells in the straight part of a tendril filament connecting the left- and right-handed parts, (d) core layer of a tendril filament (e) two cellulose fibril helices separated from the cell wall, (f) a single cellulose helix, and (g) cross section of a cellulose fibril.

the slices under SEM. The cells in L2 contain cellulose fibril helices as shown in Figure 3 (b) and (c), whereas the cells in L3 are soft and hollow tubes, with a characteristic size of 40–50 μm (Figure 3(d)). Each cell in L2 takes a tubular shape with a circular cross section of approximately 10 μm in diameter, and the circular cross section of each cellulose fibril is approximately 1–2 μm in diameter (Figure 3(e)–(f)). As shown in Figure 3(c), the helical angle of the cellulose fibril helices in the segment linking the left- and right-handed parts is significantly smaller than that in the left-handed part shown in Figure 3(f).

Discussion

Our observations indicate that helical tendrils have a hierarchy of chirality, consisting of at least six length scales from molecules, microfibrils, cellulose fibrils, cells, tendril filaments to the macroscopic tendril helix. At the molecular level, sugar units and cellulose molecules take the form of asymmetric and chiral configurations. Cellulose molecules assemble into single microfibrils at the nanoscale, which further assemble into a cellulose fibril as shown in Figure 4. At the subcellular level, the chirality occurs in the cellulose fibril helix. At the cell level, each long cell can be regarded as a chiral rod in which cellulose fibril helices exist as helical inclusions embedded in the matrix. At the tendril filament level, chirality exists in the cell bundles, i.e., chiral rod bundles. Finally, these bundles further assemble into macroscopic tendril helices with either left- or right-handedness. Therefore, the tendrils have a typical hierarchy of chirality from the molecular scale to the macroscopic scale, providing a good example for the study of chirality transfer in biological materials. The hierarchical structures of tendrils are different from those of non-chiral hierarchical materials and artificial chiral materials such as chiral polymer lamellae[20–22].

The chiral growth, as well as the swelling and deswelling processes in the experiments, involves complicated physical mechanisms of chirality transfer. The macroscopic deformation of a tendril during swelling and deswelling depends upon the features of chirality, deformation and interaction of its constituent elements at lower levels, e.g. cell bundles, cell walls, and cellulose fibril helices.

In each cell bundle, the tight cellular connections constrain the free movement and deformation of the cells. Thus the deformation of a helical tendril should be derived from the geometric and mechanical properties of the cells. As a bundle of large sized hollow cell tube, the core of tendril filament is soft. The outer layer only plays a role of protecting the inner layer and the core. In some coils of tendril helix, the outer layer can be peeled off and the tendril helix still has the

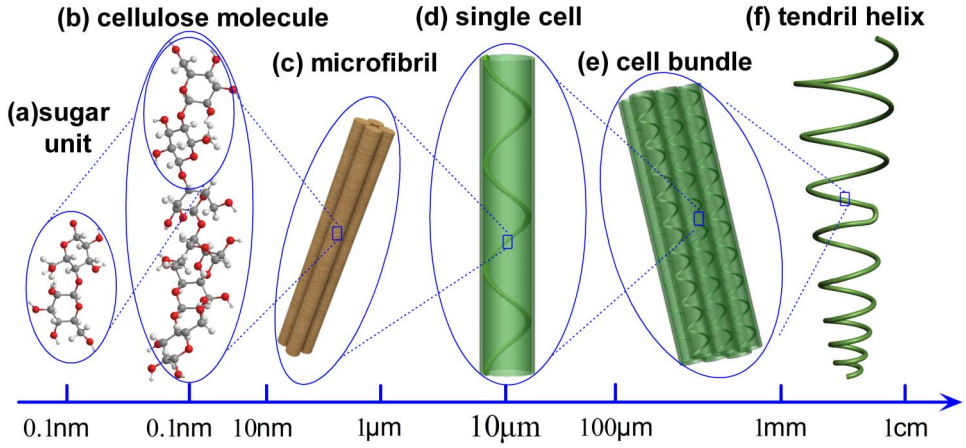

Figure 4 | Hierarchy of chirality in a tendril helix: (a) sugar unit, (b) cellulose molecule, (c) microfibril consisting of cellulose molecules, (d) single cell containing a cellulose helix, (e) cell bundle, and (f) tendril helix.

similar shape changes during the swelling and deswelling processes. This fact excludes the possibility that the out layer controls the shape changes of tendril helix. Microscopic observations in Figures 3(b) and 3(f) show that for a cell in the inner layer, the cell wall is a thin, flexible membrane assembled by polysaccharides and proteins. Thus helical cellulose fibrils should be the primary structural components of the cell. Due to the close packing of cellulose fibril helices, the cell wall can be regarded as a fiber-reinforced polymer composite, and the helical feature of ordered texture endows the cell wall with strongly orientation-dependent properties. In addition to enhancing the mechanical stiffness of the cell wall under tension, which is significant for the supporting function of tendrils, the helical structure of cellulose fibrils can also make the tendril soft and flexible upon bending, allowing the tendrils to more easily wrap around supporting objects. Thus, the cellulose fibril helices significantly affect the mechanical properties of tendrils. This structural characteristic of the inner layer cells indicates that the shape changes induced by twisting and bending deformations should be attributed to the cellulose fibril helices. Our observations of the different helical arrangements of cellulose fibrils in both the left-handed and the straight parts of a tendril also support this conclusion.

In order to further understand the microscopic mechanisms in a tendril helix, it would be of interest to compare the tendril helix with a chiral paper sheet. The twisting of paper sheets during swelling/deswelling provides another typical example of chirality transfer[23]. A twisted paper sheet is made up primarily of woody plant fibers that are glued together, and twisted paper sheets also have a hierarchy of chirality. A flat and straight swelling paper sheet can become a twisting belt because of the helical angle changes of the cellulose chain winding in the cell wall. As pointed out by Dionner et al.[23], the twisting of paper sheets also results from the helical shape changes of cellulose chains. This inspires us how the chiral structures at a lower level can induce the twisting deformation at its higher neighbor level. Unlike most woody plant cells, in which cellulose chains wind right-handed helically outside the cell wall, the inner layer cell wall of tendrils is thin, and the cellulose fibril forms a helix with left-handedness and is contained in the tendril cell wall. Moreover, the cross-sectional size of a cellulose fibril is 1–2 μm, which is much larger than the cross-sectional size of the fibrils in woody pant cells, which is only approximately 3–4 nm. Comparison of cell microstructures in tendrils and papers indicates that cellulose fibril helices play an important role during the chirality transfer process at the subcellular level.

Based on the above observations and discussions, the physical mechanisms underlying the shape changes of tendril helices during swelling and deswelling processes can be better understood. As shown in Figure 5, the typical structure of a cell in tendrils consists of a cell wall tube containing an array of cellulose fibril helices. At the fully swelled state, the cell wall tube would have a larger cross section and a relatively smaller helical angle. As the tendril gradually deswells, the radius of the cell wall cross section will decrease, corresponding to an increase in the helical angle. Thus, the cell wall would have a minimal cross-sectional radius and the cellulose fibril helix would have a maximal helical angle when the tendril is fully deswelled. The mechanical stiffness and the relatively large size of the cross section of cellulose fibril provide the cellulose fibril helix with a finite structural stiffness. During deswelling, the helical angle of cellulose fibril helices increases, leading to twisting in their morphology. Equivalently, a change in the helical angle produces a torque acting on its cross section, making the cell wall twist with either left- or right-handedness. The value of the torque depends primarily on the helical angle change at a specific swelling or deswelling state. Thus, the tendril filament will be subjected to an internal torque and undergo an intrinsic torsion, which can change the helical pitch and radius of a tendril helix during swelling or deswelling.

To rationalize the physical mechanisms underlying the formation of the helical morphology and the shape change of tendril helices, we here develop a theoretical model of tendril filaments with a spatial configuration. In this model, the effects of cellulose fibril helices at the subcellular level are taken into account. Due to the close packing of cellulose fibril helices, the cell wall is regarded as a helical and orthotropic layer. Through coordinate transformation, the constitutive relation of a tendril filament in the Frenet coordinate system of spatial curve can be written as

$$\{\boldsymbol{\sigma}'\} = [\boldsymbol{Q}']\{\boldsymbol{\varepsilon}\}_{\mathrm{FCS}}, \tag{1}$$

where $\{\sigma'\}$ and $\{\varepsilon\}_{\mathrm{FCS}}$ are the stress and the strain, respectively, and $[Q']$ is the material stiffness matrix of the tendril filament. A detailed derivation of equation (1) is given in the Supplementary Information. We assume the length and cross-sectional size of the tendril filament during swelling and deswelling keep unchanged. The helical angle of the cellulose fibril helix, α, is used to quantify the degree of swelling or deswelling of a tendril filament. The minimal and maximal values of α correspond to the fully swelled and deswelled states, respectively.

The potential energy of the tendril filament can be written as

$$\Pi = \int_0^{L_0} \left[Q_0 - Q_1\kappa(s) - Q_2\tau(s) + Q_3\kappa(s)^2 + Q_4\tau(s)^2\right] \mathrm{d}s, \tag{2}$$

where s is the arc length, $\kappa(s)$ and $\tau(s)$ denote the curvature and twist of the tendril filament, respectively. The coefficients Q_{0-4} are functions of the helical angle α of the cellulose fibril helix and are

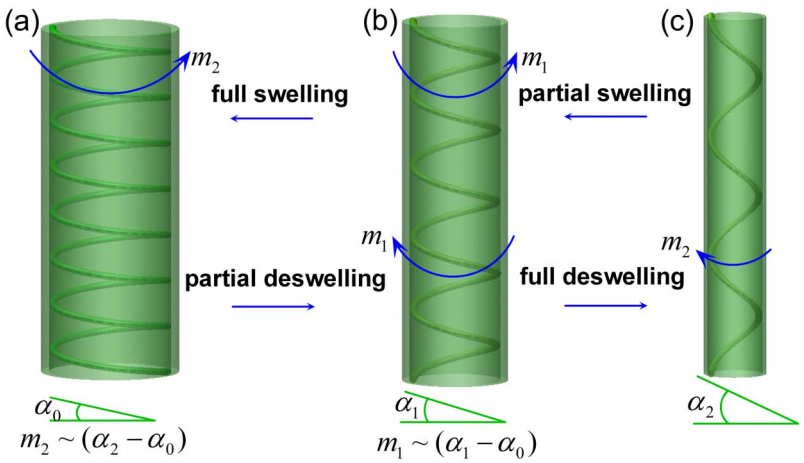

Figure 5 | Physical mechanisms of the intrinsic torsion of tendrils. (a) A fully swelled cell containing a cellulose fibril helix with the lowest value of helical angle $\alpha = \alpha_0$, (b) a partially swelled cell with $\alpha = \alpha_1 > \alpha_0$, and (c) a fully deswelled cell with the largest helical angle $\alpha = \alpha_2 > \alpha_1$.

presented in the Supplement Materials. Using the variational principle of energy[9,24,25], we can derive the following shape equation for a tendril filament with an arbitrary spatial configuration:

$$-Q_0\kappa+Q_1\tau^2-Q_2\kappa\tau+Q_3\kappa^3+(3Q_4-2Q_3)\kappa\tau^2+2Q_3\kappa_{ss} +4Q_4(\frac{\tau_s}{\kappa})\tau+Q_4\frac{2\tau_s^2}{\kappa}=0, \quad (3)$$

with $\kappa_s = d\kappa/ds$, $\tau_s = d\tau/ds$, and $\kappa_{ss} = d^2\kappa/ds^2$. For the helical shape of a tendril filament, we have $\kappa = R/(R^2+h_0^2)$ and $\tau = h_0/(R^2+h_0^2)$, where R denotes the helical radius and $h_0 = P/2\pi$, with P being the helical pitch of the tendril helix. For simplicity, assume that the helical radius and pitch of the tendril helix are constant. Then, based on equation (3), the shape equation governing the shape change of a tendril helix is rewritten as

$$Q_0R(R^2+h_0^2)^2-Q_1h_0^2(R^2+h_0^2)+Q_2Rh_0(R^2+h_0^2)-Q_3R^3 +(2Q_3-3Q_4)Rh_0^2=0. \quad (4)$$

For a helical tendril during swelling and deswelling, the helical radius R and pitch P must satisfy equation (4).

The above model allows us to predict the shape change of helical tendrils induced by swelling or deswelling. For tendril helices with different helical angles α, the helical radii and pitches calculated from equation (4) are plotted in Figure 6(a). Both the normalized helical radius and pitch decrease with the increase in α. Thus for a tendril helix during deswelling, the coil number will increase as the helical angle of the cellulose fibril helix increases because the total length of a tendril filament is approximately constant. In the case of swelling, which induces a decrease in the helical angle α of cellulose fibril helices, the shape change of tendrils can be determined easily. Figure 6(a) shows that during swelling, both the helical radius and pitch of the tendril helix increase and, therefore, its coil number decreases. In Figure 6(a), a curve PQ perpendicular to the helical angle contours is drawn to illustrate the changing tendency of the helical pitch and radius, where points P and Q are located at the curves of $\alpha = 10^\circ$ and $\alpha = 30^\circ$, respectively. Here, the curve PQ can be approximately treated as a line. Let A_1A_3 and A_2A_4 denote the projections of PQ on the two axes, respectively. It can be seen that with the decrease of the helical angle α during swelling, the helical radius increases more significantly than the helical pitch. As α changes from 30° to 10°, the helical radius and pitch increase about 16.7% and 37.7%, respectively. These results predicated by the present theoretical model have a good agreement with the experimental measurements shown in Figure 2, verifying the proposed physical mechanism of chirality transfer.

The above model reveals how the chirality at the micro scale determines the chiral shape changes at larger scales and also helps to clarify the chirality transfer of other materials with hierarchical chiral structures. It is worthy mentioning that in the proposed model, the shape change of a tendril helix results mainly from the deformation induced by the changes of chiral microstructures at the subcellular level, but the effects of chiral structural elements at lower levels (e.g., cellulose molecules) have not been considered in detail. Although cellulose molecules and their interactions have no direct influence on the mechanical properties of helical tendrils at the macroscopic scale, they do affect the mechanical behavior of cellulose fibrils and even control the handedness of cellulose fibril helices at the subcellular level. Figure 5 demonstrates that the change of the helical radius and pitch of a tendril helix during swelling/deswelling can be determined primarily by the handedness of cellulose fibril helices. Thus the chiral elements and their interactions at the molecular level may indirectly contribute to the chiral shape changes at the macro scale.

Tendril helices provide us an ideal system not only to investigate the correlation of chiralities at different length scales but also to understand the formation of helical morphologies of tendril filaments. Our experiments reveal that the deformation of tendril helices during the swelling/deswelling processes derives from the shape changes of cellulose fibril helices at the subcellular level. Similar reorientation of cellulose fibrils is also observable in growing tendrils. During the growth of tendril filaments, the growth-strain and turgor pressure may induce an elongation of cells, rendering an increase of helical angles of cellulose fibril helices and an intrinsic torsion of tendril filaments. Furthermore, intermolecular interactions also contribute to the reorientation of cellulose fibrils. For example, hemicellulose molecules in the cell walls can self-assemble in cholesteric liquid crystals, which, in turn, mediate the assembly of cellulose microfibrils into helical patterns through hydrogen bonds between hemicelluloses and cellulose chains[26,27]. During the swelling/deswelling and growth processes, some intermolecular hydrogen bonds may be broken with the appearance of water molecules[28], which may also induce the reorientation of cellulose fibrils. Thus a tendril will assume a helical shape due to the intrinsic torsion. The reorientation of cellulose fibrils drives the transfer of chirality from the molecular level to the morphological scale, as shown in Figure 4. Therefore, the shape changes of tendril helices during swelling/deswelling shed new lights on the chiral growth of tendril filaments.

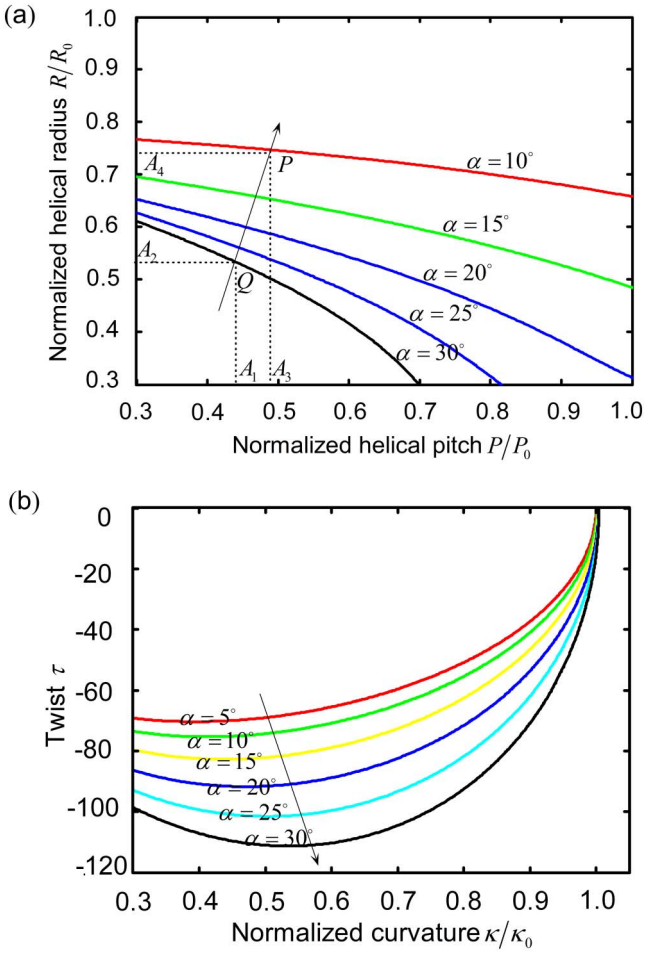

Figure 6 | (a) Helical shape variations of tendrils with respect to the helical angle α, and (b) formation and evolution of a growing tendril helix. Here, we take the cross-sectional radius of cellulose fibrils as $r_0 = 1.2 \times 10^{-6}$ m, the tendril cell radius as $r_1 = 7.0 \times 10^{-6}$ m, and the tendril radius as $r_2 = 5.0 \times 10^{-4}$ m. For the fully swelled cellulose fibril helices, the helical angle is set as $\alpha_0 = 1^\circ$ and the helical radius $R'_0 = 5.8 \times 10^{-6}$m. The elastic modulus of cellulose fibrils $E = 0.45$ GPa, and the shear modulus $G = 0.173$ GPa.

A growing tendril filament usually has a small initial curvature induced by differential growth. During the growth process, the helical angle of cellulose fibril helices gradually increases due to the increase in the turgor pressure and the growth strain, leading to an intrinsic torsion of tendril filaments, as shown in Figure 7(a). If the initially bended tendril filament has caught a support, chiral perversion may occur as a result of the intrinsic torsion. However, if no supporting object can be found, the tendril filament will twist into a helix. With the further increase of the helical angle of cellulose fibril helices, the helical pitch and radius of the tendril helix will decrease, just as in the deswelling process. According to equation (4), the variation of the helical shape of a growing tendril is plotted in Figure 6(b). In the calculation, we assume that the tendril filament has an initial curvature and a zero twist, i.e. $\kappa_0 \neq 0$ and $\tau_0 = 0$. To illustrate the efficacy of our theoretical model, Figure 7 shows the helical shape formation and evolution of a growing tendril with different helical shapes at the subcellular level. Here, our primary concern is the physical origin of the intrinsic torsion and the chirality transfer underlying the chiral growth of tendrils.

For helical tendrils and other biological materials with a hierarchy of chirality as well, growth is not only a complex process involving biochemical and physical components and structural evolutions at many different length and time scales, but also a chirality transfer process from the molecular level to the macroscopic level, as shown in Figure 4. In other words, the chirality at a lower structural level often begets a higher level chirality[29]. During the morphogenesis and remodeling process, the chirality undergoes a series of transfers from the molecular level, the cellulose fibril level, the cell level, and eventually to the macroscopic morphology of tendrils. In the theory of chirality transfer, the formation of hierarchical chiral structures at the macroscopic scale can be regarded as a consequence of multiscale chirality transfers. Here, we are primarily concerned with two issues: (i) why are the helical shapes of tendrils formed during growth, and (ii) how do they change during swelling and deswelling? In fact, both the problems involve multiscale chirality transfers.

As aforementioned, cellulose molecules have an indirect but significant influence on the chiral growth of tendrils by affecting the mechanical properties and handedness of cellulose fibrils. Although not essentially necessary for chiral growth, the chirality of cellulose molecules helps these molecules to self-assemble into cellulose fibril helices. In addition, the interactions among chiral elements at lower levels (e.g., intermolecular forces) and some other factors (e.g., growth induced residual stresses) can influence, to different extents, the chirality transfers among different length levels. Therefore, the macroscopic morphological chirality of tendrils is closely but not univocally correlated with those of cellulose fibril helices and cellulose molecules. For a tendril helix with chiral perversion, for example, the right-handed morphology is induced by an intrinsic torsion in order to compensate for the twist of its left-handed part, although the cellulose fibril helices are intrinsically left-handed. Some other climbing plants also have both right- and left-handed chiral morphologies, whereas their constituted molecules have an identical chirality.

In addition to the tendrils of climbing plants, many other biological materials, e.g., twisted tree trunks, flagellar filaments of bacteria, flower petals of Paphiopedilum dianthum and the stork's bill awns, have a hierarchy of chirality. Most of their chiral morphologies or patterns at the macro scale also derive from the chirality at the molecular, nano and micro scales, and their chiral growth usually involves a complicated process of chirality transfer. The theory of chirality transfer can help understand many interesting phenomena associated with chiral growth and establish the correlation between macroscopic morphologies and molecular structures.

In summary, we have investigated the intrinsic torsion of tendril filaments from the viewpoint of chirality transfer. Both swelling/deswelling experiments and theoretical analysis have been performed to reveal the multiscale chirality transfer mechanism underlying the chiral growth of tendrils. Based on microscopic observations of the hierarchical chiral structures of tendrils, we have developed a model to correlate the macroscopic chiral morphology and the cellulose fibril helices. Our findings may deepen our understanding of the widely observed chiral growth in biological and artificial materials. The proposed chirality transfer mechanism can also be applied to facilitate three-dimensional self-assembly and fabrication of hierarchical chiral structured materials with unique properties and functions.

Methods

(1) Swelling and deswelling experiments. Mature and dry tendril helices of left-handedness and tendril helices of opposite handednesses of *Towel Gourd* (*Tianjin*, China) were used as samples. In order to make the tendril filaments fully swelled, the samples were immersed in water for 24 hours. Then they were placed in air for 72 hours for deswelling. All tendril helices exhibited similar shape changes during swelling and deswelling, regardless of their handedness. The swelling-deswelling process was repeated four times. We measured the filament diameter, helical pitch, and radius of tendril helices at the fully swelled and deswelled states using vemier caliper with a precision of 0.01 mm.

(2) Microscopic observations. Microstructure observation of tendrils was carried out using a SEM (Hitachi SU-1500) and a field emission high-resolution SEM (JSM 6700F). The acceleration voltages of the two microscopes were set to be 30 kV and 15 kV, and their maximum resolutions were 3 nm and 1 nm, respectively. The tendril samples were coated with gold in order to enhance their conductivity.

(3) Measurement of the mechanical properties of tendrils. We determined the mechanical parameters of tendril filaments required in the theoretical analysis by tensile experiments. An electronic universal testing machine (Instron 3343) with a loading rate of 1.0 mm/min was used for this purpose. Straightened helical tendril

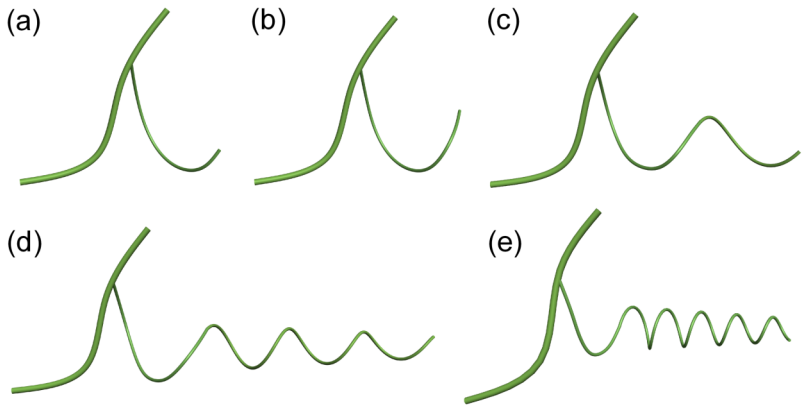

Figure 7 | Schematic diagram of the morphological evolution of a growing tendril helix. (a) The growing tendril filament with an initial curvature and zero twist, (b) the twist of the bent tendril filament induced by intrinsic torsion, (c) the formation of a tendril helix with definite curvature and twist, (c) a tendril helix with a relatively large helical radius and pitch, (d) and (e) the variations of the helical radius and the helical pitch with respect to the helical angle α.

filaments were taken as samples, and their force-displacement curves were recorded automatically. Based on the theory of composites, the mechanical properties of the tendrils were calculated from the experimental curves as Q_{11} = 0.408 GPa, Q_{22} = 0.082 GPa, Q_{12} = 0.094 GPa, and Q_{66} = 0.067 GPa.

1. Darwin, C. On the movement and habits of climbing plants (John Murray, London, 1865).
2. Isnard, S. & Silk, W. K. Moving with climbing plants from Charles Darwin's time into the 21st century. *Am. J. Bot.* **96**, 1205–1221 (2009).
3. Ye, H. M. *et al*. Surface stress effects on the bending direction and twisting chirality of lamellar crystals of chiral polymer. *Macromolecules* **43**, 5762–5770 (2010).
4. Grande, C. & Patel, N. H. Nodal signaling is involved in left-right asymmetry in snails. *Nature* **457**, 1007–1011 (2009).
5. Lough, W. J. & Wainer, I. W. Chirality in nature and applied science (Blackwell Science, Oxford, 2002).
6. Armon, S., Efrati, E., Kupferman, R. & Sharon, E. Geometry and mechanics in the opening of chiral seed pods. *Science* **333**, 1726–1730 (2011).
7. Forterre, Y. & Dumasis, J. Generating helices in nature. *Science* **333**, 1715–1716 (2011).
8. Wang, J. S., Feng, X. Q., Wang, G. F. & Yu, S. W. Twisting of nanowires induced by anisotropic surface stresses. *Appl. Phys. Lett.* **92**, 191901 (2008).
9. Wang, J. S., Ye, H. M., Qin, Q. H., Xu, J. & Feng, X. Q. Anisotropic surface effects on the formation of chiral morphologies of nanomaterials. *Proc. R. Soc. A* **468**, 609–633 (2012).
10. Chen, Z., Majidi, C., SroIovitz, D. J. & Haataja, J. Tunable helical ribbons. *Appl. Phys. Lett.* **98**, 011906 (2011).
11. Berg, H. C. & Anderson, R. A. Bacteria swim by rotating their flagellar filament. *Nature* **245**, 380–382 (1973).
12. Silverman, M. & Simon, M. I. Bacterial flagella. *Annu. Reve. Microbiol.* **31**, 397–419 (1977).
13. Calladine, C. R. Construction of bacterial flagella. *Nature* **225**, 121–124 (1975).
14. Aharoni, H., Abraham, Y., Eibaum, R., Sharon, E. & Kupferman, R. Emergence of spontaneous twist and curvature in non-Euclidean rods: application to Erodium plant cells. *Phys. Rev. Lett.* **108**, 238106 (2012).
15. Abraham, Y. *et al*. Titled cellulose arrangement as a novel mechanism for hygroscopic coiling in the stork's bill awn. *J. R. Soc. Interface* **9**, 640–647 (2012).
16. Gerbode, S. J., Puzey, J. R., McCormick, A. G. & Mahadevan, L. How the cucumber tendril coils and overwinds. *Science* **337**, 1087–1091 (2012).
17. Edwards, W., Moles, A. T. & Franks, P. The global trend in plant twining direction. *Global Ecol. Biogeogr.* **16**, 795–800 (2007).
18. Goriely, A. & Tabor, M. Spontaneous helix hand reversal and tendril perversion in climbing plants. *Phys. Rev. Lett.* **80**, 1564–1567 (1998).
19. Pieranski, P., Baranska, J. & Skjeltorp, A. Tendril perversion – a physical implication of the topological conservation law. *Eur. J. Phys.* **25**, 613–121 (2004).
20. Maillard, D. & Prud'sHomme, R. E. Crystallization of ultrathin films polylactides: from chain chirality to lamella curvature and twisting. *Macromolecules* **41**, 1705–1712 (2008).
21. Schulgasser, K. & Witztum, A. The hierarchy of chirality. *J. Theor. Biol.* **230**, 281–288 (2004).
22. Fratzl, P. & Weinkamer, R. Nature's hierarchical materials. *Prog. Mater. Sci.* **52**, 1263–1334 (2007).
23. Dionner, I., Werbowyj, R. S. & Gray, D. G. Chiral twisting curl in newsprint sheets. *J. Pulp. Pap. Sci.* **15**, J123–J126 (1991).
24. Tu, Z. C., Li, Q. X. & Hu, X. Theoretical determination of the necessary conditions for the formation of ZnO nanorings and nanohelices. *Phys. Rev. B* **73**, 115402 (2006).
25. Gao, L. T., Feng, X. Q., Yin, Y. J. & Gao, H. J. An electromechanical liquid crystal model of vesicles. *J. Mech. Phys. Solids* **59**, 2844–2862 (2008).
26. Neville, A. C. Molecular and mechanical aspects of helicoid development in plant cell walls. *BioEssays* **3**, 4–8 (1985).
27. Neville, A. C. Biology of fibrous composites (Cambridge University Press, New York, 1993).
28. Khazraji, A. C. & Robert, S. Self-assembly and intermolecular forces when cellulose and water interact using molecular modeling. *J. Nanomater.* **2013**, 1–12 (2013).
29. Wang, J. S., Feng, X. Q., Xu, J., Qin, Q. H. & Yu, S. W. Chirality transfer from molecular to morphological scales in quasi-one-dimensional nanomaterials: A continuum model. *J. Comput. Theor. Nanos.* **8**, 1278–1287 (2011).

Acknowledgements

This work was supported by the National Basic Research Program of China (Nos. 2012CB937500 and 2012CB934101), Grants-in-Aid for Scientific Research (No.21226005) from Japan Society for the Promotion of Science (JSPS) and National Natural Science Foundation of China (Nos. 11272230). J.S. thanks the supports from the JSPS research fellowship (No. P12359) and the Elite Scholar Program of Tianjin University. G.W. thanks the supports from Shanghai Pujiang Program (Nr. 11PJ1403900) and the Eastern Scholar Program at Shanghai Institutions of Higher Learning. We thank X. L. Bian and W. L. Deng for their help in the experiments.

Author contributions

J.S.W. and X.Q.F. designed and directed this study. J.S.W. carried out the experiments and theoretical simulations. G.W. carried out the microscopic observations. T.K., Y.L.K., S.W.Y. and Q.H.Q. contributed to the analysis of experimental and simulation results. All authors contributed to writing and revising the manuscript.

Additional information

Supplementary information accompanies this paper at http://www.nature.com/scientificreports

Competing financial interests: The authors declare no competing financial interests.

How to cite this article: Wang, J.-S. *et al*. Hierarchical chirality transfer in the growth of *Towel Gourd* tendrils. *Sci. Rep.* 3, 3102; DOI:10.1038/srep03102 (2013).

Supplementary Information

Hierarchical chirality transfer in the growth of *Towel Gourd* tendrils

Jian-Shan Wang[1,2*], Gang Wang[3], Xi-Qiao Feng[4†], Takayuki Kitamura[2], Yi-Lan Kang[1], Shou-Wen Yu[4], Qing-Hua Qin[5]

[1] Tianjin Key Laboratory of Modern Engineering Mechanics, Department of Mechanics, Tianjin University, Tianjin 300072, People's Republic of China

[2] Department of Mechanical Engineering and Science, Kyoto University, Nishikyo-ku, Kyoto 615-8540, Japan

[3] School of Materials Science and Engineering, Shanghai University, Shanghai 200444, People's Republic of China

[4] AML and CNMM, Department of Engineering Mechanics, Tsinghua University, Beijing 100084, People's Republic of China

[5] Research School of Engineering, Australian National University, Canberra, ACT 0200, Australia

[*] e-mail: wangjs@tju.edu.cn

[†] e-mail: Fengxq@tsinghua.edu.cn

Theoretical model

S1 Intrinsic torsion of tendril filaments

As shown in Fig. 5, the shape change of a cellulose fibril during deswelling can produce an internal torque M that acts on the cell. Following the Cosserat rod model of a spring [1, 2], the torque M can be expressed as

$$M = B'\hat{\psi}_0(\cos\alpha - \cos\alpha_0)\cos\alpha + C'\hat{\psi}_0(\sin\alpha - \sin\alpha_0)\sin\alpha\,, \tag{S1}$$

where $B' = \frac{1}{4}E\pi r_0^4$ is the bending stiffness of the tendril cell, $C' = \frac{1}{2}G\pi r_0^4$ the torsion rigidity, and $\hat{\psi}_0 = \partial\psi/\partial s = \sin\alpha_0/R_0'$, where ψ is the Euler angle, s is the arc length of cellulose fibril, R_0' is the initial helical radius of the cellulose fibril helix, r_0 is the radius of the cross section of the cellulose fibril, and α_0 and α are the helical angle of the fully swelled and partially deswelled cellulose fibril helices, respectively. Considering the cell bundle structures of the tendril filament (Fig. 4), the distributed torque m_0 acting on the tendril filament per unit length is determined as follows:

$$m_0 = \frac{Mr_2^2}{2\pi R_0' r_1^2 \tan\alpha}\,, \tag{S2}$$

where r_1 and r_2 are the radii of the cell and the tendril filament, respectively, R_0' is the helical radius of the cellulose fibril helix. During growth or swelling/deswelling of a tendril, the torque m_0 will produce an intrinsic torsion deformation of the tendrilfilament. Thus, the reorientation of cellulose fibrils provide a driving force for the formation and evolution of the tendril helix.

S2 Constitutive relationship

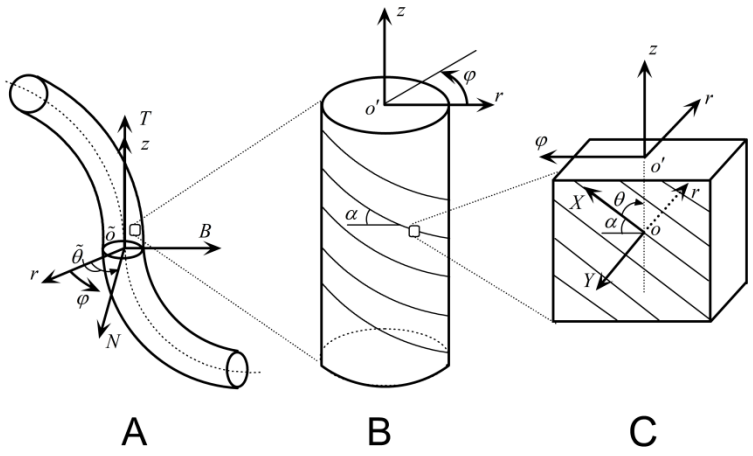

Fig. S1. Coordinate systems: (*A*) Frenet coordinate system (FCS) with base vectors $\boldsymbol{e}_N$, $\boldsymbol{e}_B$ and $\boldsymbol{e}_T$. (*B*) Cylinder coordinate system (CCS) with basis vectors $\boldsymbol{e}_r$, $\boldsymbol{e}_\varphi$ and $\boldsymbol{e}_z$; (*C*) Helical coordinate system (HCS) with basis vectors $\boldsymbol{e}_L$, $\boldsymbol{e}_T$ and $\boldsymbol{e}_r$.

In the wall of a tendril cell, cellulose fibril helices are closed packed, as shown in Fig. 3. Thus, the cell wall can be considered to be an orthotropic layer. Referring to the helical coordinate system (HCS) ($o-XYr$)shown in Fig. S1*C*, in which the X axis is oriented in the winding direction of the cellulose fibril, the r axis is oriented in the direction of the cell wall thickness, and Y is perpendicular to the X and r axes. The orthotropic layer forms a cylindrical tube that is oriented parallel to a certain direction, for which we establish the cylindrical coordinate system (CCS) ($o'-r\varphi z$). The r axis is oriented in the radial direction of the cell cylinder and the same as that in HCS, and the z and φ axes are oriented in the axial and angular directions of the cylinder, respectively. Furthermore, the tendril filament is curved into a spatial morphology and is treated here as a Kirchhoff rod having a helical microstructure. For such a spatially curved rod, we introduce a Frenet coordinate system (FCS) ($o-TBN$) shown in Fig. S1*A*, in which the origin o is located at the centerline of the tendril filament, both the z and T axes are oriented in the tangent

direction of the centerline, and the N and B axes are oriented in the normal and binormal directions of the centerline, respectively.

The constitutive relation of the helical orthotropic layer in HCS is [3]

$$\{\boldsymbol{\sigma}\}_{\mathrm{HCS}} = [\boldsymbol{Q}]\{\boldsymbol{\varepsilon}\}_{\mathrm{HCS}}, \tag{S3}$$

where $\{\boldsymbol{\sigma}\}_{\mathrm{HCS}}$ is the stress matrix and $\{\boldsymbol{\varepsilon}\}_{\mathrm{HCS}}$ is the strain matrix. The subscript HCS indicates the parameters defined in the helical coordinate system. $[\boldsymbol{Q}]$ is the orthotropic elastic stiffness matrix, which is expressed as

$$[\boldsymbol{Q}] = \begin{bmatrix} Q_{11} & Q_{12} & Q_{13} & 0 & 0 & 0 \\ Q_{12} & Q_{22} & Q_{23} & 0 & 0 & 0 \\ Q_{13} & Q_{23} & Q_{33} & 0 & 0 & 0 \\ 0 & 0 & 0 & Q_{44} & 0 & 0 \\ 0 & 0 & 0 & 0 & Q_{55} & 0 \\ 0 & 0 & 0 & 0 & 0 & Q_{66} \end{bmatrix}. \tag{S4}$$

Through coordinate transformation, we can obtain the constitutive relationship in the cylindrical coordinate system (CCS) from equation S3 as

$$\{\boldsymbol{\sigma}\}_{\mathrm{CCS}} = \left[\bar{\boldsymbol{Q}}\right]\{\boldsymbol{\varepsilon}\}_{\mathrm{CCS}}, \tag{S5}$$

where the subscript CCS stands for the parameters in the cylinder coordinate system. The stiffness matrix, $\left[\bar{\boldsymbol{Q}}\right]$, is written as

$$\left[\bar{\boldsymbol{Q}}\right] = \left[\boldsymbol{T}^{-1}\right][\boldsymbol{Q}]\left[\boldsymbol{T}^{-1}\right]^{\mathrm{T}}, \tag{S6}$$

where the subscript T denotes the transformation matrix, and

$$\left[\boldsymbol{T}^{-1}\right]=\begin{bmatrix} m^2 & n^2 & 0 & 0 & 0 & -2mn \\ n^2 & m^2 & 0 & 0 & 0 & 2mn \\ 0 & 0 & 1 & 0 & 0 & 0 \\ 0 & 0 & 0 & m & n & 0 \\ 0 & 0 & 0 & -n & m & 0 \\ mn & -mn & 0 & 0 & 0 & m^2-n^2 \end{bmatrix}, \tag{S7}$$

Here, $m=\cos\theta$, $n=\sin\theta$, and θ is the angle measured from the *L* axis to the *z* axis, and α the helical angle of a cellulose fibril. Moreover, θ and α satisfy the relationship $\theta+\alpha=90^{\circ}$.

The matrix $\left[\bar{\boldsymbol{Q}}\right]$ can obtained from equations **S6** and **S7** as follows:

$$\left[\bar{\boldsymbol{Q}}\right]=\begin{bmatrix} \bar{Q}_{11} & \bar{Q}_{12} & \bar{Q}_{13} & 0 & 0 & \bar{Q}_{16} \\ \bar{Q}_{12} & \bar{Q}_{22} & \bar{Q}_{23} & 0 & 0 & \bar{Q}_{26} \\ \bar{Q}_{13} & \bar{Q}_{23} & \bar{Q}_{33} & 0 & 0 & \bar{Q}_{36} \\ 0 & 0 & 0 & \bar{Q}_{44} & 0 & 0 \\ 0 & 0 & 0 & 0 & \bar{Q}_{55} & 0 \\ \bar{Q}_{16} & \bar{Q}_{26} & \bar{Q}_{36} & 0 & 0 & \bar{Q}_{66} \end{bmatrix}. \tag{S8}$$

A tendril filament can be regarded as an elastic rod with spatial configuration. Using coordinate transformation, we obtain the constitutive relation of tendril filaments in the Frenet coordinate system:

$$\left\{\boldsymbol{\sigma}\right\}_{\mathrm{FNT}}=\left[\boldsymbol{Q}\right]\left\{\boldsymbol{\varepsilon}\right\}_{\mathrm{FNT}}, \tag{S9}$$

where the subscript FNT indicates the Frenet coordinate system. The elastic stiffness matrix $\left[\boldsymbol{Q}\right]$ is related to $\left[\bar{\boldsymbol{Q}}\right]$ via the relation

$$\left[\boldsymbol{Q}\right]=\left[\boldsymbol{M}\right]\left[\bar{\boldsymbol{Q}}\right]\left[\boldsymbol{M}^{-1}\right] \tag{S10}$$

Here, $\left[\boldsymbol{M}\right]$ is the coordinate transfer matrix:

$$[\boldsymbol{M}]=\begin{bmatrix} 1 & 0 & 0 & 0 & 0 & 0 \\ 0 & \tilde{m}^2 & \tilde{n}^2 & 2\tilde{m}\tilde{n} & 0 & 0 \\ 0 & \tilde{n}^2 & \tilde{m}^2 & -2\tilde{m}\tilde{n} & 0 & 0 \\ 0 & -\tilde{m}\tilde{n} & \tilde{m}\tilde{n} & \tilde{m}^2-\tilde{n}^2 & 0 & 0 \\ 0 & 0 & 0 & 0 & \tilde{m} & -\tilde{n} \\ 0 & 0 & 0 & 0 & \tilde{n} & \tilde{m} \end{bmatrix} \tag{S11}$$

where $m=\cos\theta$, $n=\sin\theta$, and θ is the angle measured from the *N* axis to the *r* axis.

Since the tendril filament is very thin and slender, the strain moments on its cross-section can be approximated as constants. By averaging over the cylindrical volume ($V_0=2\pi R_0'\tan\alpha\cdot\pi R_0'^2$) containing one coil of cellulose fibril helix, the constitutive relation in equation (9) becomes

$$\{\boldsymbol{\sigma}'\}=[\boldsymbol{Q}']\{\boldsymbol{\varepsilon}\}_{\mathrm{FNT}}, \tag{S12}$$

where

$$\sigma_i'=\frac{1}{V_0}\int_0^{2\pi}\int_0^{R_0'}\int_0^{2\pi R_0'\tan\alpha}\sigma_i^{\mathrm{FNT}}r\mathrm{d}r\mathrm{d}\theta\mathrm{d}z, \tag{S13}$$

$$Q_{ij}'=\frac{1}{V_0}\int_0^{2\pi}\int_0^{R_0'}\int_0^{2\pi R_0'\tan\alpha}\tilde{Q}_{ij}r\mathrm{d}r\mathrm{d}\theta\mathrm{d}z=\frac{1}{2\pi}\int_0^{2\pi}Q_{ij}'\mathrm{d}\theta. \tag{S14}$$

Based on equation S14, we obtains

$$\begin{aligned} &Q_{11}'=\bar{Q}_{11},\quad Q_{12}'=Q_{21}'=Q_{13}'=Q_{31}'=\tfrac{1}{2}(\bar{Q}_{12}+\bar{Q}_{13}),\\ &Q_{22}'=Q_{33}'=\tfrac{1}{8}(3\bar{Q}_{22}+2\bar{Q}_{23}+3\bar{Q}_{33}),\ Q_{23}'=Q_{32}'=\tfrac{1}{8}(\bar{Q}_{22}+6\bar{Q}_{23}+\bar{Q}_{33}),\\ &Q_{44}'=\tfrac{1}{8}(3\bar{Q}_{22}+\bar{Q}_{33}-2\bar{Q}_{23}+\bar{Q}_{44}),\ Q_{55}'=Q_{66}'=\tfrac{1}{2}(\bar{Q}_{55}+\bar{Q}_{66}). \end{aligned} \tag{S15}$$

Equation S12 provides the constitutive relation of a tendril filament with the effect of cellulose fibril helices.

S3 Elastic rod model of the tendril filament

In the present study, a tendril filament with a circular cross section is treated as a Kirchhoff rod with helical microstructure. According to the Kirchhoff rod model, the strain components in the helical tendril can be expressed as [4, 5]

$$\begin{aligned}&\varepsilon_1=\varepsilon_2=0,\ \ \varepsilon_3=\omega_1 y-\omega_2 x,\ \ \gamma_{12}=\gamma_{21}=0,\\&\gamma_{13}=-\omega_1 z+\omega_3 y,\ \gamma_{23}=\gamma_{32}=\omega_3 x+\omega_1 y.\end{aligned} \tag{S16}$$

Based on equations S12 and S15, the stress components are obtained as

$$\begin{aligned}&\sigma_1=\sigma_2=0,\ \ \sigma_3=Q'_{11}(\omega_1 y-\omega_2 x),\ \ \tau_{12}=\tau_{21}=0,\\&\tau_{13}=\tau_{31}=Q'_{55}\omega_3 y,\ \ \tau_{23}=\tau_{32}=Q'_{55}(\omega_3 x+\omega_1 y).\end{aligned} \tag{S17}$$

Then, the potential energy function Π of a tendril filament of length L_0 is

$$\Pi=\int_0^{L_0}\left[H_0(\kappa(s),\tau(s))-W_0(s)\right]\mathrm{d}s, \tag{S18}$$

where $\kappa(s)$ and $\tau(s)$ are the curvature and torsion of the tendril filament, respectively. H_0 is the strain energy of the tendril filament, and W_0 the potential energy of external force, which can be written as

$$\begin{aligned}&H_0=\frac{1}{2}\left\{B(\alpha)\left[\kappa(s)-\kappa_0(s)\right]^2+C(\alpha)\left[\tau(s)-\tau_0(s)\right]^2\right\},\\&W_0=m_0(\alpha)\left[\tau(s)-\tau_0(s)\right],\end{aligned} \tag{S19}$$

where $B(\alpha)$ is the bending stiffness and $C(\alpha)$ the torsion rigidity, which are both functions of the helical angle of the cellulose fibril helix, α, and $\kappa_0(s)$ and $\tau_0(s)$ are the initial curvature and the initial torsion of the tendril filament, respectively.

equations S18 and S19 can be rewritten as

$$\Pi=\int_0^{L_0}\left[Q_0-Q_1\kappa(s)-Q_2\tau(s)+Q_3\kappa(s)^2+Q_4\tau(s)^2\right]\mathrm{d}s, \tag{S20}$$

where

$$Q_0 = \tfrac{1}{2}B(\alpha)\kappa_0^2 + \tfrac{1}{2}C(\alpha)\tau_0^2 + m_0(\alpha)\tau_0,\ \ Q_1 = B(\alpha)\kappa_0,$$
$$Q_2 = C(\alpha)\tau_0 + m_0(\alpha),\quad Q_3 = \tfrac{1}{2}B(\alpha),\ \ Q_4 = \tfrac{1}{2}C(\alpha). \tag{S21}$$

S4 Shape equations of the tendril helix

For the deformation and shape formation of a tendril filament, the equilibrium and stability of a tendril with spatial configuration require that

$$\Pi \le 0,\ \delta\Pi = 0,\ \ \delta^2\Pi \ge 0, \tag{S22}$$

where δx denotes the variation of x, and

$$\delta\Pi = \int \frac{\partial H_0}{\partial \kappa}\delta\kappa \mathrm{ds} + \int \frac{\partial H_0}{\partial \tau}\delta\tau \mathrm{ds} + \int H_0 \delta \mathrm{ds}. \tag{S23}$$

Based on equation S23 and using the calculus of variation[5-7], we obtain the following shape equations for a deformed tendril filament:

$$\begin{aligned} &-Q_0\kappa + Q_1\tau^2 - Q_2\kappa\tau + Q_3\kappa^3 + (3Q_4 - 2Q_3)\kappa\tau^2 + 2Q_3\kappa_{ss} \\ &+4Q_4(\frac{\tau_s}{\kappa})\tau + Q_4\frac{2\tau_s^2}{\kappa} = 0, \end{aligned} \tag{S24}$$

$$\begin{aligned} &-Q_1\tau_s + Q_2\kappa_s + 2(2Q_3 - Q_4)\kappa_s\tau + 2(Q_3 - Q_4)\kappa\tau_s \\ &+2Q_4\frac{\tau^2\tau_s}{\kappa} - 2Q_4(\frac{\tau_s}{\kappa})_{ss} = 0 \end{aligned} \tag{S25}$$

where $\kappa_s = \dfrac{\mathrm{d}\kappa}{\mathrm{ds}}$, $\tau_s = \dfrac{\mathrm{d}\tau}{\mathrm{ds}}$, $\kappa_{ss} = \dfrac{\mathrm{d}^2\kappa}{\mathrm{ds}^2}$, and $\tau_{ss} = \dfrac{\mathrm{d}^2\tau}{\mathrm{ds}^2}$.

For a tendril helix with a constant curvature and a constant twist, equation S25 is automatically satisfied. Thus equation S24 is rewritten as

$$\begin{aligned} &Q_0R^2 - Q_1R\sin^2\varphi + Q_2R\sin\varphi\cos\varphi - Q_3\cos^4\varphi \\ &+(2Q_3 - 3Q_4)\sin^2\varphi\cos^2\varphi = 0 \end{aligned} \tag{S26}$$

where R and φ are the helical radius and the helical angle, respectively.

For a helix, we have

$$\kappa = \frac{\cos^2\varphi}{R}, \quad \tau = \frac{\sin\varphi\cos\varphi}{R}. \tag{S27}$$

In addition, the curvature and the twist can also be expressed by the helical radius and the helical pitch as

$$\kappa = \frac{R}{R^2 + h_0^2}, \quad \tau = \frac{h_0}{R^2 + h_0^2}. \tag{S28}$$

Then the shape equation in equation S26 can be rewritten as

$$\begin{aligned} &Q_0 R(R^2 + h_0^2)^2 - Q_1 h_0^2(R^2 + h_0^2) + Q_2 R h_0(R^2 + h_0^2) - Q_3 R^3 \\ &+(2Q_3 - 3Q_4) R h_0^2 = 0 \end{aligned} \tag{S29}$$

References

1. Whitman, A. B. & DeSilva, C. N. An exact solution in a nonlinear theory of rods. *J. Elasticity* 4: 265−280 (1974).
2. Wang, J. S., Wang, G. F., Feng, X. Q. & Qin, Q. H. Surface effects on the superelasticity of nanohelices. *J. Phys. Condens. Matter* 24: 265303 (2012).
3. Marklund, E. & Varna, J. Modeling the effect of helical fiber structure on wood fiber composite elastic properties. *Appl. Compos. Mater.* 16: 245−262 (2009).
4. Liu, Y. Z. *Nonlinear mechanics of thin elastic rod: theoretical basics of mechanical model of DNA* (Tsinghua University Press, Beijing, 2006).
5. Wang, J. S., Ye, H. M., Qin, Q. H., Xu, J. & Feng, X. Q. Anisotropic surface effects on the formation of chiral morphologies of nanomaterials. *Proc. R. Soc. A* 468: 609−633 (2012).
6. Tu, Z. C., Li, Q. X. & Hu, X. Theoretical determination of the necessary conditions for the formation of ZnO nanorings and nanohelices. *Phy. Rev. B* 73: 115402 (2006).
7. Gao, L.T., Feng, X.Q., Yin, Y. J. & Gao, H. J. An electromechanical liquid crystal

model of vesicles. *J. Mech. Phys. Solids* 59: 2844-2862 (2008).